Simultaneous control of time-dependent population transfer dynamics and wave-packet quantum interferences in Li_2 by shaped ultrafast pulses

Joshua B. Ballard,* Hans U. Stauffer,* Elizabeth Mirowski, and Stephen R. Leone*
JILA, National Institute of Standards and Technology and University of Colorado, Department of Chemistry and Biochemistry, and Department of Physics, Boulder, Colorado 80309-0440
(Received 19 March 2002; published 4 October 2002)

Ultrafast pulse shapes are used to control simultaneously the optimal population transfer coefficients and rotational wave-packet quantum interferences in the $E\ ^1\Sigma_g^+$ state of Li_2 ($\nu_E=9$, $J_E=27$ and 29). By dividing the spectral bandwidth of the ultrafast pulses into multiple ''control domains'' centered on each resonant wavelength, the population transfer coefficients can be manipulated independently of the wave-packet interferences to maximize the Li_2 photoionization yield at arbitrary short pump-probe time delays. To investigate the population transfer coefficients with and without wave-packet interferences, respectively, the pump polarization is set to be either parallel to or at the magic angle ($\sim$55°) relative to the probe polarization. A comparison is made between phases that are symmetric and antisymmetric about the resonances. The effects of resonant and nonresonant frequencies are separately established and quantified. It is estimated that up to 90% of the possible nonresonant Rabi oscillations can be brought into phase simultaneously for each rovibrational state in the wave packet, while at the same time a constant phase offset added to one of the control domains establishes the phase of the wave-packet interference.

DOI: 10.1103/PhysRevA.66.043402 PACS number(s): 32.80.Qk, 33.80.Eh, 42.50.Md, 82.53.Hn

I. INTRODUCTION

Coherent control remains a primary goal of ultrafast laser dynamics studies [1,2]. Research so far addresses several key categories, such as the use of resonant frequencies to control quantum wave-packet interferences [2–5] and different pulse shapes to control multiorder processes [2,6–10]. Optimization of coherent control has been achieved using various types of learning algorithms [8,11–13], but the nature of the mechanisms for the optimal results is not always readily apparent. This paper will identify a class of pulse shapes that enhances the ground- to excited-state population transfer in a multilevel system, providing a basis for understanding the nature of optimal pulse shapes for both population transfer and quantum interferences in multilevel superpositions.

Much work has been devoted to the field of population transfer dynamics in the continuous-wave regime [14], but only recently have well-established population transfer theoretical tools been applied to the wide bandwidth inherent to ultrafast spectroscopy [13,15–18]. For example, it has been shown that chirped pulses can be used to enhance population transfer dynamics in a multiphoton process [15,19] or even in a single-photon process [13,17]. It has been shown that optimal enhancement of multiphoton dynamics can be achieved not by chirped pulses, but by applying constant phases to *blocks* of nonresonant frequencies [13,16,18]. By using a frequency-domain analysis, the optimal pulse shape is shown to depend primarily on frequencies that are near resonant, as will be discussed in detail in a later section.

This paper considers the simultaneous control of both time-dependent population transfer dynamics and superposition state quantum interferences using analytically optimal, antisymmetric pulse shapes, in comparison to simple symmetric, chirped pulse shapes and near-transform-limited pulses. Of interest are the effects of resonant and nonresonant frequencies involved in the excitation of superposition states. It analyzes the extent to which the control of the wave-packet phase influences the control of population transfer dynamics. The mutual control of wave packet and population transfer dynamics is shown to more than double the photoionization signal produced by a transform-limited pulse in a two-state superposition pump-probe experiment. A two-color ultrafast laser experimental system, with pulse shaping, is used to isolate the coherent population transfer dynamics of the two-level superposition in Li_2 molecules. The criteria for independent control of the coherent population transfer dynamics and quantum interferences are established. Extensions to more than two states are also discussed.

Simultaneous coherent control of two well-defined excited states unifies concepts concerning the dynamics between interfering superposition states and population transfer dynamics to individual states. As long as the interfering states are sufficiently separated in energy from each other, the population transfer dynamics to each state can largely be independently controlled. In Sec. II, a theoretical framework for these experiments is presented, followed in Sec. III by a description of the experimental apparatus. Finally, experimental results are presented and discussed in Sec. IV. The degree to which the population transfer for two states can be independently controlled is included in that final section.

II. THEORY

In the weak-field limit, first-order time-dependent perturbation theory can be used to describe a single-photon absorption. The excited-state amplitude coefficient for a single state

*Present address: Department of Chemistry and Department of Physics, University of California, and Lawrence Berkeley National Laboratory, Berkeley, CA 94720.

is described in the time domain [20]:

$$c_n(t)=\frac{\mu_{eg}}{i\hbar}\int_{-\infty}^{t}\varepsilon(t)\exp(i\omega_{eg}t')dt', \tag{1}$$

where μ_{eg} is the dipole moment matrix element between the excited and ground states, $\varepsilon(t)$ is the electric field as a function of time, and $\omega_{eg}=(E_e-E_g)/\hbar$ is the transition frequency. As shown in [16,18,21], this excited-state amplitude can be approximated for positive time t by the frequency-domain expression

$$c_n(t)=\frac{\mu_{eg}}{i\hbar}\left\{\tilde{\varepsilon}^*(\omega_{eg})-\frac{i}{\pi}\wp\int_{-\infty}^{\infty}\frac{\varepsilon(\omega)\exp[i(\delta)t]}{\delta}d\omega\right\}, \tag{2}$$

where $\tilde{\varepsilon}^*(\omega_{eg})$ is the amplitude of the electric field at the transition frequency, $\varepsilon(\omega)$ is the amplitude of light at frequency ω, $\delta=\omega-\omega_{eg}$ is the detuning, and $\wp$ is the Cauchy principal value. The first term in Eq. (2) represents the resonant contribution to the excited-state amplitude, and the second term represents nonresonant contributions. As t approaches infinity, the second term averages to zero, and Eq. (2) reduces to the resonant component; however, the second term does not necessarily average to zero for small t (i.e., within the pulse width). In the absence of any phase manipulation (i.e., transform-limited pulses), the nonresonant term will be greatly diminished for all t, since the δ term for $\omega > \omega_{eg}$ is of opposite sign relative to that for $\omega < \omega_{eg}$ [18]. Additionally, the i/π leading factor of the nonresonant term places the nonresonant contribution $\pi/2$ out of phase with the resonant term. This phase relationship suggests that, to bring all frequency components into phase at small t an additional $+\pi/2$ and $-\pi/2$ phase must be added to the nonresonant frequencies above and below ω_{eg}, respectively. Additionally, the $1/\delta$ dependence of the nonresonant term shows that the most influential frequencies will be those with the smallest detuning. These results may then be generalized to multiple states.

The $1/\delta$ dependence of the nonresonant wavelengths lends itself to the possibility that frequencies with a large δ can be manipulated with minimal influence on the excited-state coefficient dynamics. This will allow for the manipulation of multiple states, provided that the energy separation between states, $\Delta\omega$, is great enough that all frequencies near one state have little effect on any other states. In the discussion below, we use ''control domain'' to refer to large blocks of wavelengths surrounding each resonant transition and ''resonant control domain'' or ''resonance'' to refer to very small bandwidth regions centered on each resonant transition.

Lithium dimer (Li_2) is used as a model system to investigate the extent to which nonresonant frequencies can be used to control multiple excited-state coefficients with a single pulse. The relevant potential energy curves in Li_2 are shown in Fig. 1 [22–24]. From a single launch state, two rovibrational states ($\nu_E=9$, $J_E=27$ and 29) are accessible within the bandwidth of the pump laser, creating a time-dependent wave packet. A probe pulse ionizes the coherent superposition at various pump-probe time delays to obtain

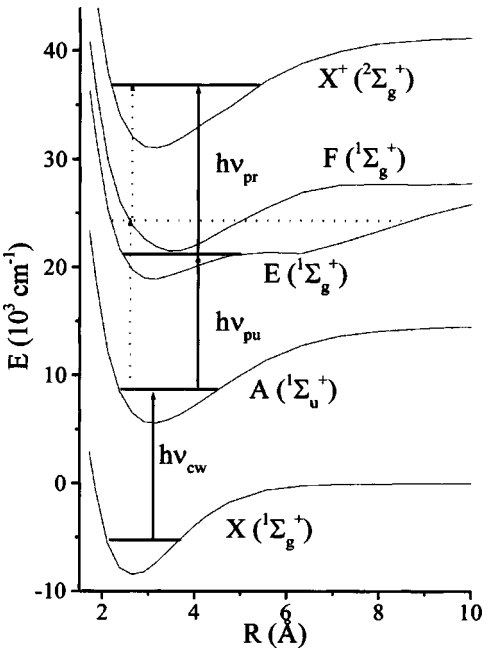

FIG. 1. Relevant potential energy curves. A cw laser excites from the $X\ ^1\Sigma_g^+$ electronic curve to a pure launch state on $A\ ^1\Sigma_u^-$. An 800 nm ultrafast laser excites a superposition of states on the $E\ ^1\Sigma_g^+$ curve, which is subsequently ionized by a time-delayed 640 nm ultrafast probe pulse. At negative delays, the probe-pump pathway through the $F\ ^1\Sigma_g^+$ state, as indicated by the dotted lines, has a much lower yield than the positive time pathway due to unfavorable Frank-Condon overlap factors.

the signal. For parallel pump and probe polarizations (referred to as a ''parallel probe''), the presence of multiple rotational states in the wave packet produces a coherent superposition state with oscillations at a frequency equal to the energy difference between the states [25]:

$$S(t)\cong|pr_1|^2|c_1(t)|^2+|pr_2|^2|c_2(t)|^2 +2|pr_1pr_2||c_1(t)c_2(t)|\cos[\Delta\omega t+\Delta\varphi(t)], \tag{3a}$$

where pr_1 and pr_2 are constants related to the probe step (not discussed here); the energy separation $\Delta\omega$ is 42 cm^{-1} (1.5 THz); and $\Delta\varphi$ is the relative phase between the wave-packet states at time t. It has been shown that for a probe polarization oriented at the magic angle ($\sim$55°) with respect to the pump polarization (''magic-angle probe''), the coherent oscillation is completely suppressed, so

$$S(t)=|pr_1|^2|c_1(t)|^2+|pr_2|^2|c_2(t)|^2, \tag{3b}$$

because the coherent oscillation is rotational in nature [6,24]. Hence, by manipulating the probe polarization, we can select whether the signal reflects a full wave-packet trace or simply the ground- to excited-state population transfer dynamics. Furthermore, by subtracting the magic-angle probe signal from the parallel probe signal, we are left with just the coherent oscillation piece

$$S(t)=2|pr_1pr_2||c_1(t)c_2(t)|\cos(\Delta\omega t+\Delta\varphi). \quad (3c)$$

The probe step consists of an ultrafast pulse of a different color from the pump pulse [26]. This aspect of the signal acquisition was not considered above for simplicity. The color of the probe pulse is chosen so that the probability for a probe-pump (i.e., $t<0$) ionization pathway is below the noise level, allowing time-dependent ionization to occur only at positive time delays. There is a constant background component to the photoionization signal at all time delays, and this has also been subtracted out of the signals. Hence, the observed photoionization signal only shows the time-dependent coefficient buildup behavior and the quantum interference of the superposition state as described in Eq. (4).

III. EXPERIMENT

The lithium sample is contained in a heat pipe at 1050 K and is photoionized by a three-step excitation process. An overview of the laser system is given below, but details can be found in previous work [13,26]. In this experiment, a narrow-bandwidth continuous-wave (cw) laser, an ultrafast amplifier system, and an optical parametric amplifier (OPA) are used, and all but the OPA are pumped by a 27 W argon ion laser. The frequency of the cw laser is tuned to a specific $A\ ^1\Sigma_u^+ \leftarrow X\ ^1\Sigma_g^+$ resonance (606.954 nm) of Li_2, producing a pure launch state ($\nu_A=11$, $J_A=28$) on the first excited electronic potential energy curve. The ultrafast regenerative amplifier is seeded by a 76 MHz oscillator to produce 180 fs [full width at half maximum (FWHM)] ultrafast pulses at a 200 kHz repetition rate, $\sim$ 800 nm central wavelength with 8 nm (FWHM) bandwidth. These ultrafast pulses are split into two beams, with 25% of the light becoming the pump pulse and 75% of the light frequency doubled to pump the OPA. The resulting 15 mW OPA output is a train of nearly transform-limited pulses with a 200 fs FWHM pulsewidth and a central wavelength of 640 nm. The OPA output is variably time delayed relative to the pump pulse via a precision delay stage.

To shape the pump pulse, it is sent through a dispersion free pulse shaper [27,28]. In the pulse shaper's Fourier plane, a liquid-crystal spatial light modulator (SLM) is used to shape the spatially dispersed pump light by independently attenuating and/or applying phase to 128 individual frequency components (SLM pixels) of the pump light. The central frequencies imaged onto the SLM pixels are separated by approximately 4 cm^{-1} with a single-frequency spot size of approximately 1.7 pixels. Normally, the 8 nm FWHM pulses are imaged onto the SLM to achieve a bandwidth of 40 pixels FWHM.

The cw laser, pump, and probe pulses intersect in the interaction region in the center of the heat pipe. The ions are produced between two parallel plates separated by 1 cm with a 10 V potential applied across the interaction region. The cw light is optically chopped, and the resulting current is detected with a lock-in amplifier that is synchronized to the cw modulation.

To study the effects of nonresonant frequencies, two classes of pulse shape have been used to enhance transient photoionization effects, shown in Fig. 2. The first class has a symmetric phase shape about each resonance that has been shown to transiently enhance excited-state coefficients [17] (''chirp-type spectrum''). It consists of a quadratic phase applied across the frequency spectrum around each resonance with the form $\varphi(\omega)=c\,\delta^2+\varphi_k$, where $\delta=\omega_i-\omega$ is the detuning from the nearest resonance, and φ_k is a constant phase [see Fig. 2(a)]. The constant phase φ_k is applied to the entirety of one of the control domains to control the phase of the wave-packet interferences. An antisymmetric phase mask for population transfer comprises the second class, called the ''phase-jump spectrum''; this phase mask involves the application of $\pi/2$ and $-\pi/2$ rad above and below resonance, as established in several recent works [see Fig. 2(b)] [16,18]. The resonant portion of the control domain is defined here as a block of two pixels ($\sim$8 cm^{-1} FWHM) centered on a specific transition, chosen to avoid attenuating the long-time-delay signal by diffraction [13]. So, in effect, ''resonance'' actually refers to the smallest practical bandwidth achievable by our pulse shaper around each transition. As in the case of the chirp-type spectrum, the relative phase of the wave-packet states using the phase-jump spectrum is manipulated by adding a constant phase to only one of the control domains. It must be noted that, in each of the cases above, the phase-mask profiles for both control domains is the same, assuring the same population transfer dynamics for each state in the superposition. Additionally, this will assure that the

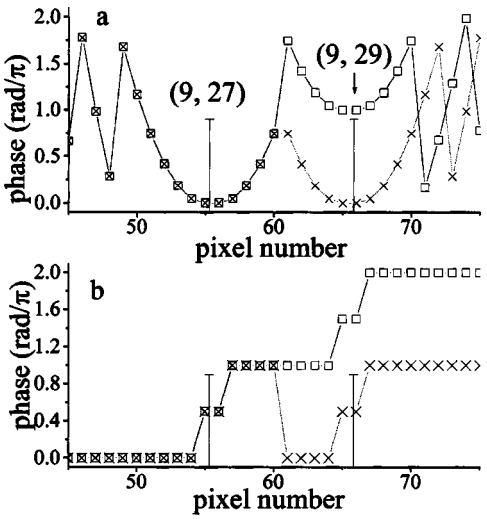

FIG. 2. Phase-mask classes used in this article. In both panels, quantum state resonances ($\nu_E=9$, $J_E=27$ and 29) are marked with vertical lines. Relative phase offsets of 0.0 and π rad between control domains are represented by crosses ($\times$) and squares ($\square$), respectively. (a) Chirp-type spectra. The degree of quadratic phase, c, is defined by $\varphi(\text{pixel})=c(\delta_{\text{pixel}})^2$ where δ_{pixel} is the separation in pixels from the nearest resonance. (b) Phase-jump spectra. A phase of $+\pi/2$ and $-\pi/2$ is added to the frequencies above and below resonance, respectively. A linear phase of $\varphi(\text{pixel})=c\,\delta_{\text{pixel}}$ is added to the phase masks to induce a time shift in the population transfer (not shown). The phase on pixel 56 is always the same as that on pixel 55, and the phase on pixel 66 is always the same as that on pixel 65.

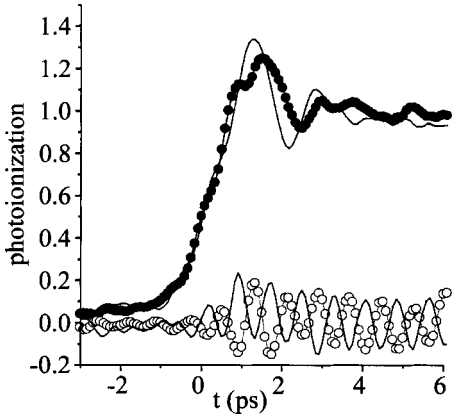

FIG. 3. Chirp-type pump spectrum transients. The upper solid line and circles (●) represent the magic-angle probe transient for π and 0 rad relative phase between control domains, respectively, and a chirp factor of 0.2. The lower solid line and circles (○) represent just the coherent oscillations produced with the same phase masks as above.

wave-packet phase will remain nearly constant during the population transfer process.

IV. RESULTS AND DISCUSSION

This section will first analyze the ability to control quantum beats while applying a previously studied chirp-type phase mask around each state, but extended to a quantum superposition. Next it will be shown that the phase-jump spectrum gives a much greater enhancement in the transient photoionization, by up to a factor of 2 for a wave-packet phase shift of π. Finally, the nonresonant contributions to the photoionization will be compared to a simple model to quantify the degree to which the quantum states in the superposition can be independently controlled.

To demonstrate the separability of the population transfer dynamics from the wave-packet oscillations, we first examine the previously studied case of the chirp-type spectrum [17], with results for the two states at the magic angle [Eq. (3b)] and parallel probe minus the magic angle [Eq. (3c)], shown in Fig. 3. The population transfer dynamics in the upper part of the figure show several traits of the buildup produced by a strictly chirped pulse. After time zero, there is a peak in the excited-state population followed by a short period of ringing. After just a few picoseconds, this ringing decays, leaving a constant value for the excited-state population. Notice that these characteristics are present for both zero and π relative phase between the control domains, and in both cases there is a peak in the excited-state population around a planned delay time of 1.2–1.3 ps, depending on the degree of chirp, in this case a 0.2 chirp factor. The coherent oscillations, which are simply the difference between the parallel and magic-angle probes, are also predictably controlled. Clearly, a π phase shift of one coherent oscillation relative to the other can be induced during the entire population transfer process, which is simply a result of adding π phase to only one of the resonant control domains. Additionally, around 1.2 ps, the amplitude of the coherent oscillations passes through

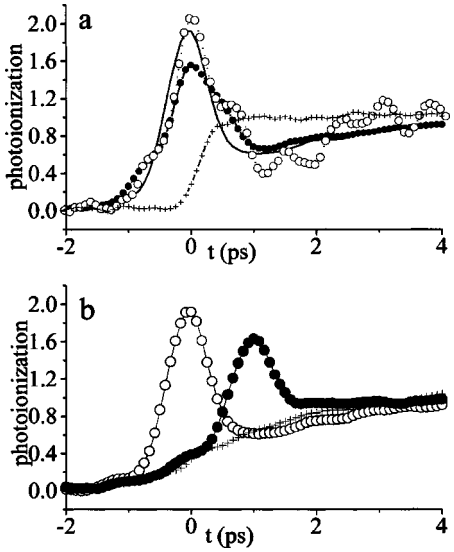

FIG. 4. Phase-jump pump spectrum transients. (a) Magic-angle probe traces produced using zero phase offset (●) and π phase offset (solid line) between the control domains, and parallel probe photoionization signal (○) for zero control domain phase offset. A trace produced by an unshaped pump pulse (+) is included for reference. (b) Population transfer traces produced by adding a simple phase pattern to the phase-jump spectrum, with π phase offset between wave-packet resonances. Linear phase was added to nonresonant frequencies to time-shift the peak photoionization by 0.0 and 1.0 ps (○ and ●, respectively). The crossed line (+) represents an attempt to shift the nonresonant contribution to a time beyond the capabilities of the experimental apparatus, resulting in a purely resonant excitation effect.

a maximum, as expected from Eq. (4a). The combination of the population transfer dynamics and the wave-packet interferences produces a clear peak in the photoionization signal at 1.2 ps despite the slightly decreased population transfer using zero phase offset between control domains.

The analysis of the chirp-type spectrum above establishes that both the population transfer dynamics and wave-packet interferences can be independently controlled. This section now explores more optimal phase masks to maximize the photoionization due to the population transfer dynamics in conjunction with the interference of two states at specific short pump-probe time delays.

Several magic-angle and parallel pump-probe data are summarized in Fig. 4(a). A pump-probe transient obtained with the phase-jump spectrum of Fig. 2 clearly shows an enhancement in the excited-state population, in addition to the proper phasing of the coherent oscillation at $t=0$, shown in Fig. 4(a). Two population transfer traces (magic-angle probe) are shown, along with a total wave-packet signal (parallel probe) that is designed to have a maximum in the quantum beat at the same delay (0.0 ps) as the maximum in the population transfer. The population transfer traces use phase masks with 0 and π relative phase between two control domains, and the full wave-packet signal is set to have 0 relative phase between the two control domains [the ×'s in Fig. 2(b)]. Both population transfer traces show a peak at the same pump-probe time delay, with the case of π relative

phase between control domains [the □'s in Fig. 2(b)] having the larger peak amplitude by 15%.

Of all relative phases between control domains of the phase-jump class, the case of zero relative phase is the least optimal for population transfer. This is so because all of the wavelengths between the two wave-packet states in one control domain maximally destructively interfere with the buildup of the other control domain. For example, the light on pixels 57–60 [in the (9,27) domain] maximally destructively interferes with the buildup of state (9,29), where the control domain includes pixels 61–128. Even so, the wave-packet interference produces a global maximum in the photoionization at 0.0 ps pump-probe delay.

In Fig. 4(b) several population transfer traces are shown for the phase-jump spectra with different amounts of linear phase added just to the nonresonant frequencies; these traces are generated using only π relative phase between the wave-packet resonances. Evident in this figure is that for each trace there is a slow, monotonic buildup (>4 ps) of population attributable to resonant (and very near resonant) frequencies coupled with a much shorter time-scale population transfer attributable to nonresonant frequencies. The nonresonant contributions to the population transfer show peak widths between 750 and 790 fs FWHM. These data will be used later to quantify the degree to which the superposition states can be independently controlled.

The phase-jump spectrum permits a higher degree of coherent control than the chirp-type spectrum as shown by the fact that at short times the phase-jump spectrum doubles the excited-state population, whereas the chirp-type spectrum shows a maximum of 30% improvement of the photoionization signal. The phase-jump spectrum shows greater population transfer enhancement than the chirp-type spectrum because the phase-jump shape assures that all nonresonant contributions come into phase simultaneously. This is in contrast to the chirp-type situation, in which only certain nonresonant contributions are in phase at any one time.

The mechanism for the increase in population transfer for the phase jump spectrum can be attributed to off-resonant Rabi oscillations. In the weak-field limit, the Rabi frequency $\Omega(\delta)=\{\delta^2+[\mu_{eg}\varepsilon(\delta+\omega_{eg})/\hbar]^2\}^{1/2}$ reduces to $\Omega(\delta)=\delta$, since $[\mu_{eg}\varepsilon(\delta+\omega_{eg})]^2 \ll \delta^2$ for values of δ with non-negligible electric-field amplitudes [14]. Additionally, given that the amplitude of any nonresonant oscillation is proportional to $\varepsilon(\delta+\omega_{eg})/\delta$ [29], the total of all nonresonant contributions to the excited-state populations can then be formulated as $c(t)\propto\int_{-\infty}^{\infty}d\delta[\varepsilon(\delta+\omega_{eg})/\delta]^2\sin^2[\delta t/2+\phi(\delta)]$. Notice the similarity of this representation to Eq. (2). To bring all of these sine waves into phase at $t=0$, a phase mask with $+\pi/2$ and $-\pi/2$ rad applied to the positive and negative detuned wavelengths, respectively, must be implemented. At the resonant wavelength (i.e., where $\delta=0$), the optimal phase will be intermediate between the positive and negative detuning, or zero degrees. Thus we have the same optimal phase pattern as predicted by Eq. (2). In contrast, for the chirped-phase pattern, not all nonresonant Rabi oscillations come into phase simultaneously. Rather, there is a series of partial recurrences in time; this is observed as a ringing in the signal.

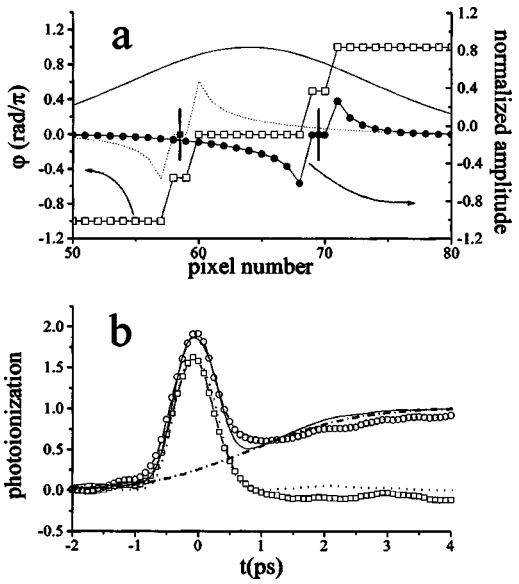

FIG. 5. Comparison of model results with experiment. (a) Phase (□) and amplitude (●) [$\varepsilon(\omega_p)/\delta_p$ from Eq. (5)] of the oscillations created by each pixel used to generate the nonresonant contribution to the model population transfer dynamics. Resonances are marked with vertical lines, and the electric-field spectrum is given by the solid line. A second state (dashed line) is included for reference. (b) Comparison of model and experiment. The experimental nonresonant (□) and full population transfer traces (○) are compared to the model nonresonant (dotted line) and full population transfer (solid line) traces. The model resonant contribution is given by the dot-dashed line.

To quantify the degree to which the two states in the experiments described here can be independently manipulated, a model based upon Eqs. (1) and (2) is implemented. This model accounts for the nonresonant and resonant contributions to the signal and is summarized in Fig. 5. Equation (2) is used to account for the nonresonant contributions to the population transfer:

$$c_n(t)=\frac{\mu_{eg}}{h}\sum_p \frac{\varepsilon(\omega_p)\exp[i(\delta_p)t-i\varphi_p]}{\delta_p}, \qquad (4)$$

where the summation is over all pixels (p) of the SLM, with each pixel representing light of a specific frequency ω_p and phase φ_p. In essence, each pixel creates an oscillation with frequency δ_p and amplitude $\varepsilon(\omega_p)/\delta_p$. Transform-limited pulses with Gaussian spectral widths equal to experimental observations are assumed, giving $\varepsilon(\omega_p)$, and the quantum states are assumed to be symmetrically located under the spectral envelope. In Fig. 5(a), the values of $\varepsilon(\omega_p)/\delta$ and φ_p are plotted. The amplitude of the light at the two pixels around each resonance is assumed to be zero here, but it is accounted for in the resonant portion of the model. The signal is then computed as a convolution of the excited-state population $|c_n(t)|^2$ with a 180 fs FWHM Gaussian probe pulse. The model population transfer dynamics fit very well with the experimental data, as shown in Fig. 5(b).

Given the good agreement between model and experiment, a more quantitative analysis of the interaction between

control of wave-packet phase and population transfer dynamics is given below. For a two-state superposition, a lower limit of the degree to which the population transfer to state *i* can be independently controlled, I_{PT_i}, is quantified as

$$I_{\mathrm{PT}_i}=1-2n\left|\int_{\Delta\omega/2}^{+\infty}d\delta'\,\varepsilon(\delta_i')/\delta_i'\right|^2, \tag{5}$$

where $\Delta\omega$ is the difference in energy between the superposition states ($\Delta\omega=\omega_i-\omega_j$), the second limit of integration ($\pm\infty$) has the same sign as $\Delta\omega$, and $\varepsilon(\delta')$ is the amplitude of the electric field at a specific detuning. The factor of 2 accounts for destructive interference, and *n* normalizes the expression. Physically speaking, I_{PT_i} is a measure of the cumulative intensity of all nonresonant contributions to a particular population at a specific time relative to the ideal case (i.e., single control domain). In the case where two states have degenerate energies (i.e., $\Delta\omega=0$) with a uniform energy spectrum $I_{\mathrm{PT}}=0$, the states cannot be independently controlled. On the other hand, in the limit of $\Delta\omega=\pm\infty$, the second term goes to zero, and the states can be controlled completely independently of each other ($I_{\mathrm{PT}}=1$). This analysis assumes a regime where the spectrum is divided into an arbitrary number of ''control domains,'' with a specified bandwidth devoted to the control of each state. The spectrum is divided into two or more regions, and the integrated value of $e(\delta_i')/\delta_i'$ inside the control domain for state *i* is compared to $e(\delta_i')/\delta_i'$ outside its control domain. Increasing the number of states involved in a control scheme will likely decrease the spectral width of the control domain for any state, decreasing the degree to which that state can be independently controlled. Using Eq. (4) to quantify the influence of nonresonant frequencies, Eq. (5) shows that each state can be controlled up to 90% independently (i.e., $I_{\mathrm{PT}_i}=0.90$).

The resonant contribution to the signal is modeled using Eq. (1). The electric field is assumed to be transform limited with a bandwidth for excitation equal to approximately 10 cm^{-1} FWHM, which corresponds to the light imaged onto two pixels. Each quantum state is assumed to be located at the central frequency of its respective narrow bandwidth region to best mimic experiment and to minimize computational artifacts related to the singularity at $\delta=0$. This component of the modeled signal shows a slow, monotonic increase in the excited-state population, just as one would expect from a several picosecond transform-limited pulse. When the resonant and nonresonant components of the model are added together, they closely follow the experimental signal, as shown in Fig. 5(b). A similar analysis was performed on the results using phase-jump spectra with 0 rad relative phase, with similar outcomes, further supporting the validity of this model. In future work, the effects of changing the energetic spacing between states will be used to experimentally verify the bandwidth considerations presented earlier.

We have shown the ability to independently implement the coherent control of both the population transfer coefficients and quantum interferences to two states in a superposition. Additionally, we have shown that the optimal pulse shape for transient population transfer in the weak-field regime is characterized by nonresonant wavelengths that are shifted by $\pi/2$ and $-\pi/2$ rad relative to the resonant wavelengths. Using a simple model based upon the assumption that an ultrafast transition can be described by a collection of driven oscillators, we have quantified the degree to which the two states in the superposition can be independently controlled. This work should be instrumental for designing coherent control pulse schema and for understanding solutions found by various learning algorithms.

ACKNOWLEDGMENTS

The authors gratefully acknowledge the support of the National Science Foundation.

[1] R. J. Gordon and S. A. Rice, Annu. Rev. Phys. Chem. **48**, 601 (1997).
[2] H. Rabitz, R. de Vivie-Riedle, M. Motzkus, and K. Kompa, Science **288**, 824 (2000).
[3] M. Shapiro and P. Brumer, J. Chem. Phys. **84**, 4103 (1986).
[4] A. H. Zewail, G. Casati, S. A. Rice, M. Chergui, D. J. Tannor, T. Kobayashi, and H. Rabitz, Adv. Chem. Phys. **101**, 3 (1997).
[5] N. F. Scherer, D. M. Jonas, and G. R. Fleming, J. Chem. Phys. **99**, 153 (1993).
[6] M. Gruebele and A. H. Zewail, J. Chem. Phys. **98**, 883 (1993).
[7] L. Zhu, K. Suto, J. A. Fiss, R. Wada, T. Seideman, and R. J. Gordon, Phys. Rev. Lett. **79**, 4108 (1997).
[8] M. Bergt, T. Brixner, B. Kiefer, M. Strehle, and G. Gerber, J. Phys. Chem. **103**, 10 381 (1999).
[9] R. Bartels, S. Backus, E. Zeek, L. Misoguti, G. Vdovin, I. P. Christov, M. M. Murnane, and H. C. Kapteyn, Nature (London) **406**, 164 (2000).
[10] R. J. Levis, G. M. Menkir, and H. Rabitz, Science **292**, 709 (2001).
[11] T. C. Weinacht, Ph.D. thesis, University of Michigan, 2000.
[12] T. Hornung, R. Meier, and M. Motzkus, Chem. Phys. Lett. **326**, 445 (2000).
[13] J. B. Ballard, H. U. Stauffer, Z. Amitay, and S. R. Leone, J. Chem. Phys. **116**, 1350 (2002).
[14] W. Demtroder, *Laser Spectroscopy*, 2nd ed. (Springer, Berlin, 1998).
[15] J. Cao, C. J. Bardeen, and K. R. Wilson, J. Chem. Phys. **113**, 1898 (2000).
[16] N. Dudovich, B. Dayan, S. M. Gallagher Faeder, and Y. Silberberg, Phys. Rev. Lett. **86**, 47 (2001).
[17] S. Zamith, J. Degert, S. Stock, B. d. Beauvoir, V. Blanchet, M. A. Bouchene, and B. Girard, Phys. Rev. Lett. **87**, 033001 (2001).
[18] D. Oron, N. Dudovich, D. Yelin, and Y. Silberberg, Phys. Rev. Lett. **88**, 063004 (2002).
[19] V. V. B. Yakovlev, C. J. Bardeen, J. W. Che, J. Cao, and K. R. Wilson, J. Chem. Phys. **108**, 2309 (1998).
[20] M. Shapiro, J. Phys. Chem. **97**, 7396 (1993).

[21] J. Paci, M. Shapiro, and P. Brumer, J. Chem. Phys. **109**, 8993 (1998).
[22] I. Schmidt-Mink, W. Muller, and W. Meyer, Chem. Phys. **92**, 263 (1985).
[23] A. Pashov, W. Jastrzebski, and P. Kowalczyk, J. Chem. Phys. **113**, 6624 (2000).
[24] J. M. Papanikolas, R. M. Williams, P. D. Kleiber, J. L. Hart, C. Brink, S. D. Price, and S. R. Leone, J. Chem. Phys. **103**, 7269 (1995).
[25] R. Uberna, M. Khalil, R. M. Williams, J. M. Papanikolas, and S. R. Leone, J. Chem. Phys. **108**, 9259 (1998).
[26] R. A. Uberna, Z. Amitay, C. X. W. Qian, and S. R. Leone, J. Chem. Phys. **114**, 10 311 (2001).
[27] H. Kawashima, M. M. Wefers, and K. A. Nelson, Annu. Rev. Phys. Chem. **46**, 627 (1995).
[28] M. M. Wefers and K. A. Nelson, Opt. Lett. **18**, 2032 (1993).
[29] L. Allen and J. H. Eberly, *Optical Resonance and Two-Level Atoms*, 2nd ed. (Dover, New York, 1987).